Laser-assisted electron scattering in strong-field ionization of dense water vapor by ultrashort laser pulses

2014 New J. Phys. 16 083032

(http://iopscience.iop.org/1367-2630/16/8/083032)

New Journal of Physics
The open access journal at the forefront of physics
Deutsche Physikalische Gesellschaft DPG | IOP Institute of Physics

Laser-assisted electron scattering in strong-field ionization of dense water vapor by ultrashort laser pulses

M Wilke[1], R Al-Obaidi, A Moguilevski, A Kothe, N Engel, J Metje, I Yu Kiyan[1] and E F Aziz[1]

Joint Ultrafast Dynamics Lab in Solutions and at Interfaces (JULiq), Helmholtz-Zentrum Berlin, Albert-Einstein-Str. 15, 12489 Berlin and Freie Universität Berlin, FB Physik, Arnimallee 14, 14195 Berlin, Germany
E-mail: martin.wilke@helmholtz-berlin.de, igor.kiyan@helmholtz-berlin.de and emad.aziz@helmholtz-berlin.de

Received 1 April 2014, revised 21 May 2014
Accepted for publication 11 June 2014
Published 14 August 2014

New Journal of Physics **16** (2014) 083032

doi:10.1088/1367-2630/16/8/083032

Abstract

We report on strong-field ionization of dense water gas in a short infrared laser pulse. By employing a unique combination of photoelectron spectroscopy with a liquid micro-jet technique, we observe how the character of electron emission at high kinetic energies changes with the increase of the medium density. This change is associated with the process of laser-assisted electron scattering (LAES) on neighboring particles, which becomes a dominant mechanism of hot electron emission at higher medium densities. The manifestation of this mechanism is found to require densities that are orders of magnitude lower than those considered for heating the laser-generated plasmas via the LAES process. The experimental results are supported by simulations of the LAES yield with the use of the Kroll–Watson theory.

Keywords: strong laser field, photoionization, electron scattering

[1] Authors to whom any correspondence should be addressed.

1. Introduction

The strong-field light–matter interaction has received great attention during the past few decades. Ionization is one of the fundamental processes which has been studied in detail at the elementary level of the field interaction with isolated atoms or molecules [1, 2]. Generation of hot electrons represents a characteristic feature of this process at high laser intensities. The energy scale is typically expressed in terms of the ponderomotive energy U_p of a free electron undergoing a quiver motion in the field. For a linearly polarized field it has the form $U_p = F^2/4\omega^2$, where F and ω are the electric field strength and the laser frequency, respectively (atomic units are used throughout unless else specified). It is well known that the spectrum of electrons emitted directly to the continuum in the process of above-threshold ionization (ATI) extends up to kinetic energies of $2U_p$. The high-order ATI occurs due to rescattering of the direct electron on the parent core in the presence of the laser field. Its spectrum has a cutoff energy of approximately $10U_p$ [1, 2]. As an example, for a laser intensity of 10^{15} W cm^{-2} and a photon energy of 1 eV this cutoff lies at 1.4 keV.

Much higher kinetic energies of photoelectrons can be reached from the interaction of condensed matter with strong laser fields of similar intensities. The collective absorption of radiation by an ionized ensemble of atoms or molecules results in a higher energy deposition per particle. In general, a plasma created at the leading edge of the laser pulse is considered as the radiation absorber during the interaction of the ionized medium with the rest of the pulse. The absorption efficiency of the optically created plasma represents a hot topic related to the possibilities to develop plasma-based x-ray lasers [3] and to initiate nuclear fusion of the heated ions [4].

The induced inverse bremsstrahlung is one of the driving mechanisms of plasma heating [5]. This process, also called laser-assisted electron scattering (LAES), was first predicted a few decades ago [6] and recently received much attention in view of its high rate in intense laser fields and its similarity to the high-order ATI process [7–9]. The LAES effect has a nonlinear character and consists in multiphoton absorption (or emission) of laser radiation by electrons scattered off plasma particles. The plasma heating rate due to the LAES process is proportional to the frequency of collisional events, which is dependent on the medium density. It was considered that rather high densities, in the order of 10^{19} cm^{-3}, are needed for this mechanism to be essential on a femtosecond time scale [10, 11]. Therefore, investigation of the LAES process with the use of ultrashort laser pulses represents a challenging task if a diluted gas medium is used [12].

In the short-pulse regime, several different effects leading to efficient absorption of radiation and generation of hot electrons were considered on a mesoscopic scale. They are attributed to a finite size of the created plasma or, in general, to the presence of a boundary. This is the case for ionization of clusters, nanoparticles, droplets, or ionization from the surface of a solid state. Some of these effects are vacuum heating [13], generation of the ignition field [14, 15], electron scattering at the inner cluster boundary [5], resonant excitation of collective electron dipole oscillations [16, 17], and near-field electron acceleration at the surface of a dielectric [18].

In the present work we reexamine the efficiency of the LAES process in the short-pulse regime. Using ultrashort laser pulses, we show that this process can result in emission of hot electrons from a uniform medium where the geometrical confinement of molecules is not predefined. Water vapor is used as a sample. The electron acceleration due to the LAES effect

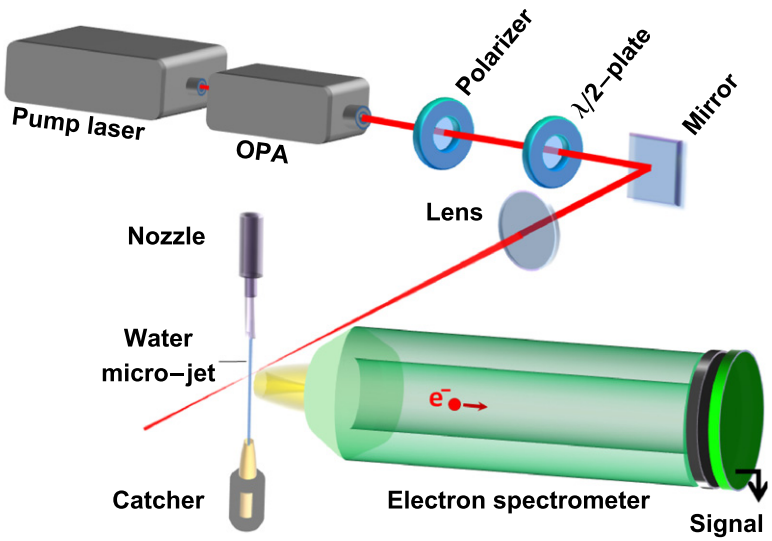

Figure 1. Schematic view of the experimental setup.

manifests itself in angle resolved energy spectra of photoelectrons, which we record at different vapor densities by employing time-of-flight (TOF) electron spectroscopy. We observe a large energy gain by photoelectrons, significantly exceeding the energy cutoff of high-order ATI, which occurs already at moderate densities in the range above 10^{15} cm^{-3}. This value is orders of magnitudes lower than the density previously considered for the efficiency of plasma heating [10, 11].

2. Experimental procedure

The experimental setup is illustrated in figure 1. Linearly polarized infrared laser pulses of 1450 nm wavelength were generated in an optical parametric amplifier (OPA) pumped with a Ti: sapphire laser at a repetition rate of 5 kHz. In order to avoid saturation of the detector by the large amount of electrons generated in the dense gas, the pulse energy was attenuated down to 40 μJ with the use of a polarizer. The laser beam was focused by a spherical lens into the interaction region in front of the TOF electron spectrometer. The focus spot size of 26 μm (FWHM) and the pulse duration of 38 fs (FWHM), corresponding to 8 optical cycles, were measured with the use of beam diagnostic tools. These parameters yield the peak intensity in the laser focus of approximately 1.3×10^{14} $W\,cm^{-2}$, giving rise to the ponderomotive energy of 25.6 eV.

The design and performance characteristics of the TOF spectrometer are presented in detail in [19]. In the present experiment, the spectrometer was operated in the field-free configuration, i.e., without imposing a magnetic field onto the interaction region to increase the collection efficiency of photoelectrons. The entrance into the drift tube was equipped with a skimmer of 100 μm size, which enabled us to maintain high-vacuum conditions inside the spectrometer during the experiment. Electrons that passed through the drift tube were multiplied by means of a double stack of micro-channel plates (MCP) and collected by a phosphor screen that served as an anode. The amplified signal was recorded by using a time-to-digital converter card. The spectrometer scale was previously calibrated in a broad energy range, extending up to 1000 eV,

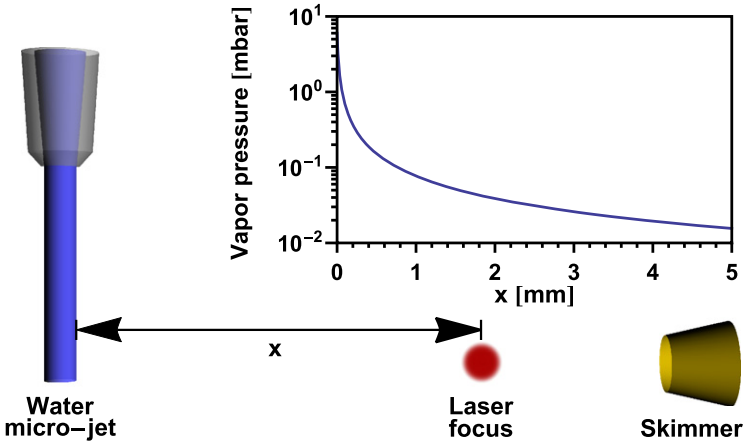

Figure 2. Geometry of the interaction region. The inset plot shows the vapor pressure dependency on the distance from the micro-jet surface, calculated by using of equation (1).

by using synchrotron radiation of the BESSY II light source [19]. For the field-free configuration of the spectrometer, the acceptance angle of photoelectrons is approximately 1.1 °. This value constituted the angular resolution in the present experiment. Positioning the spectrometer axis perpendicular to the laser beam propagation direction facilitated measurement of angular distributions of photoelectrons by rotating the polarization axis of the laser beam with the use of a half-wave plate.

The vapor density variation in the interaction region was accomplished by creating a water filament in the experimental vacuum chamber with the use of a liquid micro-jet technique [20]. This technique consists in pumping liquid through a nozzle with a small diameter, which results in the formation of a jet exhibiting a laminar flow of a few millimeters in length before it becomes turbulent. In the laminar region the jet represents a liquid rod with a diameter defined by the nozzle size. A nozzle of 20 μm diameter was used in the present experiment. According to the model developed by Faubel [21], the vapor pressure in the vicinity of a micro-jet is inversely proportional to the radial distance R from the jet center:

$$P = \frac{R_0}{R} P_0 \left(R \geqslant R_0\right), \tag{1}$$

where R_0 is the radius of the micro-jet and P_0 is the equilibrium pressure at its surface. Thus, by decreasing the distance between the jet and the laser focus from 10 mm to 20 μm (where the two beams nearly intersect), the vapor pressure in the interaction region was varied by approximately three orders of magnitude. Its upper value of 6 mbar corresponded to the equilibrium vapor pressure at a water surface with a temperature of 0 °C.

The water jet was oriented perpendicular to the laser beam and centered in front of the spectrometer skimmer. The laser focus was kept at a fixed position in front of the skimmer and closer to the skimmer than the jet (see figure 2 for illustration). In the experimental routine, we first optimized the photoelectron signal generated by the emission from the liquid phase. Doing so provided the reference for the central overlap of the laser beam and the micro-jet. This routine had a precision on the order of 2 μm. Afterwards, the distance between the micro-jet and the focus was set by translating the nozzle perpendicular to the laser beam with a precision of

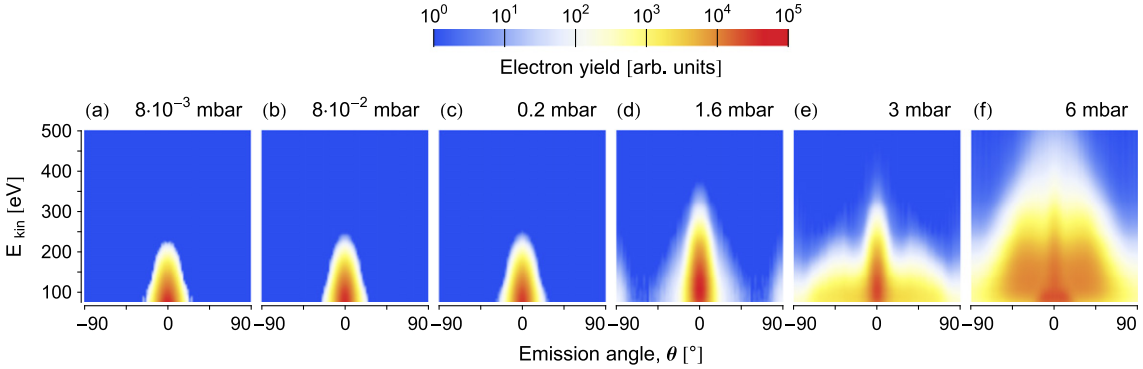

Figure 3. Experimental emission spectra of water vapor. The emission angle θ is given with respect to the laser polarization axis. E_{kin} denotes the electron kinetic energy. The spectra are obtained for different vapor pressures: (a) 8×10^{-3} mbar, (b) 8×10^{-2} mbar, (c) 0.2 mbar, (d) 1.6 mbar, (e) 3 mbar and (f) 6 mbar. The signal in the individual images is normalized to the corresponding vapor density.

1 μm. The combined uncertainty in the jet positioning was therefore much smaller than the focus size and the jet diameter. A catcher collected water downstream of the jet and thus facilitated pumping of the experimental chamber. The residual vapor pressure in the chamber was approximately 5×10^{-5} mbar, which represents the lowest pressure value applied in the experiment.

3. Results and discussion

In the present study we focused on the emission of energetic electrons with kinetic energies exceeding 60 eV. In this energy range, the rescattering effects dominated the photoelectron yield and thus their contribution could be easily distinguished from the contribution of direct ionization, which has the classical energy cutoff of $2U_p \simeq 51.2$ eV. Due to the much lower count rate of rescattered electrons compared with the signal of direct electrons, the detector was not saturated at energies above 60 eV. It is also important to note that the high-energy part of the spectrum was not affected by the space charge effect because the fast electrons left the interaction region before a significant charge was cumulated.

Figure 3 shows a series of angle-resolved energy spectra of photoelectrons recorded for different distances between the jet and the laser focus. The corresponding pressure values, lying in the range between 8×10^{-3} and 6 mbar, were obtained from the measured distances by using equation (1) and taking the jet size of 20 μm into account. One can see that the shape of the photoelectron spectrum does not change with the increase of pressure up to approximately 0.2 mbar. Here each distribution exhibits electron emission at small angles with respect to the laser polarization axis and with kinetic energies extending to approximately 230 eV. This is also demonstrated in figure 4, which shows the kinetic energy distributions at the emission angle $\theta = 0°$. The distributions are normalized to the corresponding pressure values. One can see that at lower vapor pressures (8×10^{-3}, 8×10^{-3}, and 0.2 mbar) the normalized spectra resemble each other. Their cutoff energy of 230 eV corresponds to the value of $10U_p$ calculated at the peak laser intensity. Thus, the three distributions shown on the left-hand side of figure 3 demonstrate the signal of the rescattered electrons generated in the high-order ATI process.

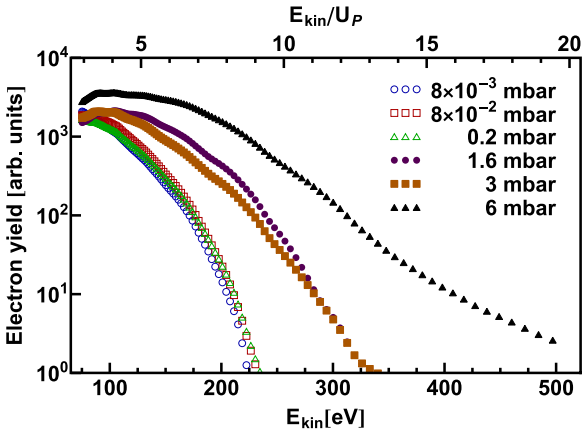

Figure 4. Kinetic energy distributions along the laser polarization direction recorded at different vapor pressures. The spectra are normalized to the corresponding pressure values.

The emission spectrum undergoes a tremendous change in the pressure range above 0.2 mbar. It reveals the contribution of electrons with significantly higher kinetic energies (see figure 4) as well as at large angles with respect to the laser polarization. In the following discussion, we demonstrate that these effects are due to the LAES process, which involves scattering of electrons, generated by direct ionization, onto the neighboring gas particles.

Before discussing the LAES effect in detail, let us consider the possible contributions of other processes that occur in a strong laser field. As demonstrated in [22], ionization of the laser-dissociated fraction of water molecules has a low yield under the short-pulse condition. The laser pulse duration applied in the present study is comparable to the pulse duration used in [22]. Therefore, we neglect the contribution of the dissociation process. Even if dissociation would be efficient, the sequential ionization of the dissociation products cannot lead to the increase of the high-energy cutoff beyond the semiclassical value. The formation of water clusters due to evaporation from the jet surface is unlikely because it requires a break of many hydrogen bonds. Thus, evaporation of single molecules determines the medium in the vicinity of the laminar jet, which is experimentally confirmed in [23, 24]. Multiple ionization of water molecules also cannot be responsible for the spectral cutoff exceeding the semiclassical value of $10U_p$. Since the yield of multiple ionization is typically much lower than the yield of single ionization [25], we do not take it into account in the present work.

To describe the LAES-process, we first consider the condition required for a scattering event to take place in the time interval of the laser pulse duration. Assuming that the target gas is an ideal gas with a temperature of 0 °C, one can calculate that at a pressure of 0.2 mbar the density of water molecules is $\sim 5 \times 10^{15}$ cm^{-3}, corresponding to the mean free path of 60 nm between particles. Photoelectrons with a kinetic energy of approximately 6 eV or higher overcome such a distance within the pulse duration of 38 fs and can thus initiate a subsequent LAES event on a neighboring molecule. This energy requirement is fulfilled in the direct ionization process, which has a cutoff energy of 51.2 eV. However, similar estimations show that if the gas pressure is below 10^{-2} mbar, the energy requirement lies beyond this cutoff value.

One should note that the yield of direct electrons is maximal at kinetic energies considerably lower than $2U_p$ and is exponentially small at the cutoff energy. For the laser field

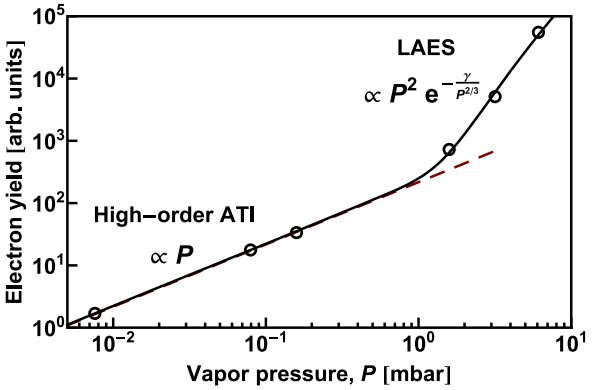

Figure 5. Total yield of high-energy electrons plotted as a function of vapor pressure. The dashed line shows the linear dependency of the high-order ATI signal. The solid line represents a combined fit to both the linear and the non-linear empirical dependency introduced in the text.

parameters used in the present experiment, the maximum lies below 5 eV according to the simulations of direct ionization presented later. Therefore, the value of 0.2 mbar can be considered as the critical gas pressure for the LAES process to occur.

In the preceding discussion we did not consider the scattering condition for electrons generated in the high-order ATI process. Since the yield of this process is typically several orders of magnitude lower than the yield of direct electrons [1], we disregard the LAES of high-order ATI electrons in our consideration.

The preceding consideration of the critical vapor pressure is supported by the results shown in figure 5, where the total yield of high-energy electrons is plotted against the vapor pressure. The yield was integrated over electron kinetic energies in the range $E_{kin} \geqslant 75$ eV and over emission angles $-90° \leqslant \theta \leqslant 90°$. The weighting factor $\sin\theta$ was taken into account in the integration over θ because of the axial symmetry of photoelectron distributions with respect to the laser polarization direction. Figure 5 reveals different dependencies of the yield in the given pressure range. At lower vapor densities, where the high-order ATI process constitutes the signal, the total yield is linearly proportional to the pressure (note the double logarithmic scale in the figure). With increasing pressure, the dependency becomes non-linear.

Since the LAES yield is proportional to both the gas density and the density of electrons undergoing the scattering process, it is expected to obey a quadratic dependency on the pressure, assuming that the scattering condition and the scattering rate are the same for all electrons generated in the ionization step. However, the scattering condition and the rate are energy dependent and, therefore, are non-uniform within the energy distribution of ionized electrons. More specifically, as the vapor density increases, a larger amount of slower electrons is involved in the LAES process. We find that an empirical function $P^2 \cdot \exp(-\gamma/P^{2/3})$ can be used to describe the total yield at higher pressure values. Here γ is a numerical constant, and the exponential function describes the fraction of ionized electrons for which the scattering condition discussed above is satisfied. It is assumed that the energy distribution of ionized electrons exponentially decreases as a function of the kinetic energy, and the dependency of the LAES rate on the electron kinetic energy is disregarded. The solid line in figure 5 represents a combined fit to both the linear and non-linear empirical dependencies. One can see that the

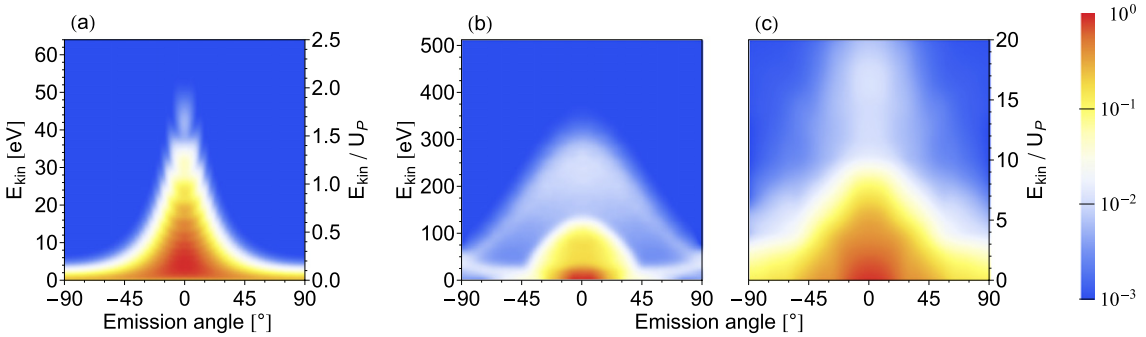

Figure 6. Calculated emission spectra. Simulations are performed for (a) direct ionization, (b) single-step LAES process, and (c) double-step LAES process.

electron yield deviates from the linear dependency on the pressure in the range above 0.8 mbar, which is on the same order of magnitude as the critical value of 0.2 mbar estimated previously.

We now present results of simulations of photoelectron spectra formed in the LAES process. The aim of presenting these simulations is to demonstrate the major changes in the energy and angular distributions of the direct electrons due to the LAES effect. We do not intend to provide a quantitative description of the experimental spectra, which would require a comprehensive consideration of the dynamics of different processes within the laser pulse duration as well as knowledge of their absolute rates. One should also note that the spectrum shown in figure 3(f) was recorded with the laser focus close to the jet surface and, therefore, ionization of liquid water partially contributed to the signal. The much higher density of molecules in the liquid phase gives rise to a high probability of multiple scattering events. A sequence of two LAES events will be considered in the following discussion. Comparing contributions to the signal from the gas and the liquid phase for the case when the laser focus is centered at the jet surface is worthwhile. Despite the large difference (approximately 5 orders of magnitude) in medium density at the surface and in the bulk, the partial yields of electrons collected from gas and from liquid are comparable due to the geometry of the interaction/collection region. Indeed, on the one hand the region of laser interaction with vapor extends over a much longer distance along the laser propagation direction, and electron collection in this dimension is limited by the skimmer size of 100 μm (to be compared with the jet size of 20 μm). On the other hand, electrons generated in bulk water cannot easily leave the medium. Their effective attenuation length (EAL) of 2 nm [26] defines the thickness of a surface layer from which the electrons can be collected (to be compared with the focus size of 26 μm). This consideration concerns the spectrum shown in figure 3(f). The signal in other spectra was dominated by ionization of the gas phase.

As a starting point, the spectrum of direct ionization shown in figure 6(a) was simulated by using predictions of theory based on the strong-field approximation [27]. The experimental laser field parameters, the H_2O ionization potential of 12.6 eV [28], and the *p*-character of the highest-occupied molecular orbital of the water molecule were taken into account in the simulation. Calculations were performed according to the routine described in detail in [29].

The spectrum of electrons that experienced the subsequent LAES event was calculated by using the predictions by Kroll and Watson for the differential LAES cross section [6]:

$$\frac{d\sigma_n(\mathbf{k}, \mathbf{k}_i)}{d\Omega_{\mathbf{k}}} = \frac{k}{k_i} J_n^2\left(\hat{\mathbf{e}}_{\mathrm{L}} \cdot (\mathbf{k}_i - \mathbf{k})\frac{F}{\omega^2}\right)\frac{d\sigma_{\mathrm{el}}}{d\Omega}, \tag{2}$$

where $\mathbf{k}_i$ and $\mathbf{k}$ represent the electron momenta before and after the scattering event, n is the number of absorbed or emitted photons, $\hat{\mathbf{e}}_{\mathrm{L}}$ is the unit vector along the laser field polarization, J_n is the Bessel function, and $d\sigma_{\mathrm{el}}/d\Omega$ is the field-free elastic scattering differential cross section. The initial and final electron momenta satisfy the energy conservation condition $k^2/2 = k_i^2/2 + n\omega$. The LAES spectrum was obtained by integrating equation (2) over the initial momentum distribution of direct electrons, $dW_i(\mathbf{k}_i)/d\Omega_{\mathbf{k}_i}$ and by adding up contributions from different n-photon channels:

$$\frac{dW(\mathbf{k})}{d\Omega_{\mathbf{k}}} = \sum_n \int_{\mathbf{k}_i} \frac{dW_i(\mathbf{k}_i)}{d\Omega_{\mathbf{k}_i}} \frac{d\sigma_n(\mathbf{k}, \mathbf{k}_i)}{d\Omega_{\mathbf{k}}}\, d\mathbf{k}_i. \tag{3}$$

The distribution $dW_i(\mathbf{k}_i)/d\Omega_{\mathbf{k}_i}$ is given by the spectrum shown in figure 6(a), transformed to the momentum scale. Evaluation of equation (3) was carried out with the use of a Monte Carlo routine. The electron yield was averaged over the spatiotemporal intensity distribution in the laser focus. The LAES yield was calculated by assuming that the scattering event occurs at the same local intensity as the direct ionization. Due to the conditions required for scattering events to occur, the incident kinetic energy $E_i = k_i^2/2$ was considered to be in the range above 6 eV. In this range the inequality $E_i \gg \omega$ is satisfied and, thus, the validity criterion of the Kroll–Watson approximation is fulfilled. The field-free differential cross section $d\sigma_{\mathrm{el}}/d\Omega$ was obtained from the available experimental data [30, 31] by interpolating the cross section values given for a discrete set of incident electron energies and scattering angles. The interpolation was performed by using cubic splines.

The simulated spectrum due to a single LAES event is presented in figure 6(b). It demonstrates a significant energy gain of direct electrons that reaches a value of 10 U_p, which is analogous to the energy cutoff of the high-order ATI process [32]. We find that higher kinetic energies are obtained when electrons are scattered back with respect to their incident direction. The contribution of such events is pronounced in the spectrum shown in figure 6(b) as demonstrated by the distinct cone structure that embraces the yield of forward-scattered electrons with lower energies. In contrast to the high-order ATI yield, which is localized along the laser polarization direction, the LAES angular distribution appears rather broad and has a prominent contribution at 90 $^\circ$ with respect to the laser polarization axis. These features are consistent with the observed changes in photoelectron spectra at higher gas densities (see figure 3(d–f)). We would like to note that our simulations reveal a similar angular dependency of the LAES energy cutoff as recently reported in [7].

Due to the large increase in kinetic energy, the scattered electrons can undergo a sequence of LAES events before the laser intensity diminishes to zero. At each step of this sequence, electrons gain an additional energy which, in turn, facilitates the scattering condition for the subsequent step. As an example, figure 6(c) shows a spectrum of electrons that experienced a second LAES event. The spectrum was obtained by repeating the calculation routine with the use of the spectrum shown in figure 6(b) as the initial distribution of incident electrons. The simulation reveals an additional increase of the cutoff energy by $10U_p$. This result reproduces well the spectrum shown in figure 3(f) reflecting the high probability of LAES processes in a dense medium. One should note that the yield of high-order ATI electrons and their LAES process should also be taken into account for a quantitative description of the experimental spectra.

It is interesting to point out that the cutoff energy can be used to judge the number of sequential LAES events experienced by photoelectrons. One can see from figure 4 that the spectra obtained at 1.6 and 3 mbar pressure extend to the same kinetic energy. Also, the shapes of these two normalized distributions is not much different, similar to the case of high-order ATI spectra recorded at lower gas densities (see figure 4). These results indicate that for both 1.6 and 3 mbar pressure the scattering condition allows only one LAES event to occur. The tremendous increment of the cutoff energy in the spectrum recorded at 6 mbar is due to the increase in the number of sequential scattering events.

4. Summary

The observations reported here provide a bridge between studies of elementary processes in strong laser fields and studies of collective effects in the interaction of light with condensed matter. The results demonstrate how the elementary LAES process, which is insignificant in the diluted phase, becomes prominent in the condensed phase. The application of ultrashort laser pulses emphasizes the LAES effect, since other mechanisms leading to the plasma heating are inertial and can be discriminated due to the short interaction time. The present study demonstrates the efficiency of collective energy deposition to a uniform medium of moderate density due to the LAES process. This demonstration provides an essential step in understanding plasma effects in liquid and solid states. The developed method can be applied to investigate the interaction of strong laser fields with liquid interfaces.

Acknowledgments

This work is funded by European Research Council grant no. 279344 and by the Helmholtz-Gemeinschaft via the VH-NG-635 grant.

References

[1] Dimauro L and Agostini P 1995 *Adv. At. Mol. Opt. Phys.* **35** 79
[2] Becker W, Grasbon F, Kopold R, Milošević D B, Paulus G and Walther H 2002 *Adv. At. Mol. Opt. Phys.* **48** 35
[3] Dunn J, Osterheld A L, Shepherd R, White W E, Shlyaptsev V N and Stewart R E 1998 *Phys. Rev. Lett.* **80** 2825
[4] Ditmire T, Zweiback J, Yanovsky V P, Cowan T E, Hays G and Wharton K B 1999 *Nature* **398** 489
[5] Krainov V and Smirnov M 2002 *Phys. Rep.* **370** 237
[6] Kroll N M and Watson K M 1973 *Phys. Rev.* A **8** 804
[7] Čerkić A and Milošević D B 2013 *Phys. Rev.* A **87** 033417
[8] Milošević D B, Paulus G G, Bauer D and Becker W 2006 *J. Phys. B: At. Mol. Opt. Phys.* **39** R203
[9] Flegel A V, Frolov M V, Manakov N L and Starace A F 2009 *Phys. Rev. Lett.* **102** 103201
[10] Rae S C and Burnett K 1992 *Phys. Rev.* A **46** 2077
[11] Ditmire T, Donnelly T, Rubenchik A M, Falcone R W and Perry M D 1996 *Phys. Rev.* A **53** 3379
[12] Kanya R, Morimoto Y and Yamanouchi K 2010 *Phys. Rev. Lett.* **105** 123202
[13] Brunel F 1987 *Phys. Rev. Lett.* **59** 52
[14] Snyder E M, Buzza S A and Castleman A W Jr 1996 *Phys. Rev. Lett.* **77** 3347
[15] Rose-Petruck C, Schafer K J, Wilson K R and Barty C P J 1997 *Phys. Rev.* A **55** 1182

[16] Shao Y L, Ditmire T, Tisch J W G, Springate E, Marangos J P and Hutchinson M H R 1996 *Phys. Rev. Lett.* **77** 3343
[17] Schlipper R, Kusche R, von Issendorff B and Haberland H 1998 *Phys. Rev. Lett.* **80** 1194
[18] Zherebtsov S *et al* 2011 *Nat. Phys.* **7** 656
[19] Kothe A, Metje J, Wilke M, Moguilevski A, Engel N, Al-Obaidi R, Richter C, Golnak R, Kiyan I Y and Aziz E F 2013 *Rev. Sci. Instrum.* **84** 023106
[20] Faubel M, Steiner B and Toennies J P 1997 *J. Chem. Phys.* **106** 9013
[21] Faubel M, Schlemmer S and Toennies J 1988 *Z. Phys. D* **10** 269
[22] Mathur D, Rajgara F A, Dharmadhikari A K and Dharmadhikari J A 2008 *Phys. Rev.* A **78** 023414
[23] Mafuné F, Takeda Y, Nagata T and Kondow T 1992 *Chem. Phys. Lett.* **199** 615
[24] Morgner H, Oberbrodhage J and Wulf M 1993 *J. Electron Spectrosc. Relat. Phenom.* **61** 183
[25] Eichmann U, Dörr M, Maeda H, Becker W and Sandner W 2000 *Phys. Rev. Lett.* **84** 3550
[26] Thürmer S, Seidel R, Faubel M, Eberhardt W, Hemminger J C, Bradforth S E and Winter B 2013 *Phys. Rev. Lett.* **111** 173005
[27] Gribakin G F and Kuchiev M Y 1997 *Phys. Rev.* A **55** 3760
[28] Tan K, Brion C, der Leeuw P V and van der Wiel M 1978 *Chem. Phys.* **29** 299
[29] Bergues B, Ansari Z, Hanstorp D and Kiyan I Y 2007 *Phys. Rev.* A **75** 063415
[30] Cho H, Park Y S, Tanaka H and Buckman S J 2004 *J. Phys. B: At. Mol. Opt. Phys.* **37** 625
[31] Danjo A and Nishimura H 1985 *J. Phys. Soc. Japan* **54** 1224
[32] Paulus G G, Becker W, Nicklich W and Walther H 1994 *J. Phys. B: At. Mol. Opt. Phys.* **27** L703